water

MDPI

Article

Extension of Iber for Simulating Non–Newtonian Shallow Flows: Mine-Tailings Spill Propagation Modelling

Marcos Sanz-Ramos [1,*], Ernest Bladé [1], Martí Sánchez-Juny [1] and Tomasz Dysarz [2]

[1] Flumen Research Institute, Polytechnique University of Catalonia (UPC)—International Centre of Numerical Method in Engineering (CIMNE), 08034 Barcelona, Spain; ernest.blade@upc.edu (E.B.); marti.sanchez@upc.edu (M.S.-J.)

[2] Department of Hydraulic and Sanitary Engineering, Faculty of Environmental Engineering and Mechanical Engineering, Poznań University of Life Sciences, 60-649 Ponzan, Poland; tomasz.dysarz@up.poznan.pl

* Correspondence: marcos.sanz-ramos@upc.edu

Abstract: Mine tailings are commonly stored in off-stream reservoirs and are usually composed of water with high concentrations of fine particles (microns). The rupture of a mine-tailings pond promotes, depending on the characteristics of the stored material, the fluidization and release of hyper-concentrated flows that typically behave as non–Newtonian fluids. The simulation of non–Newtonian fluid dynamics using numerical modelling tools is based on the solution of mass and momentum conservation equations, particularizing the shear stress terms by means of a rheological model that accounts for the properties of the fluid. This document presents the extension of Iber, a two-dimensional hydrodynamic numerical tool, for the simulation of non–Newtonian shallow flows, especially those related to mine tailings. The performance of the numerical tool was tested throughout benchmarks and real study cases. The results agreed with the analytical and theoretical solutions in the benchmark tests; additionally, the numerical tool also revealed itself to be adequate for simulating the dynamic and static phases under real conditions. The outputs of this numerical tool provide valuable information, allowing researchers to assess flood hazard and risk in mine-tailings spill propagation scenarios.

Keywords: numerical modelling; Iber; viscous-plastic flows; gypsum tailings; pyroclastic/pyritic tailings

check for updates

Citation: Sanz-Ramos, M.; Bladé, E.; Sánchez-Juny, M.; Dysarz, T. Extension of Iber for Simulating Non–Newtonian Shallow Flows: Mine-Tailings Spill Propagation Modelling. *Water* **2024**, *16*, 2039. https://doi.org/10.3390/w16142039

Academic Editors: Ruiping Liu and Youning Xu

Received: 17 June 2024
Revised: 8 July 2024
Accepted: 16 July 2024
Published: 18 July 2024

Copyright: © 2024 by the authors. Licensee MDPI, Basel, Switzerland. This article is an open access article distributed under the terms and conditions of the Creative Commons Attribution (CC BY) license (https://creativecommons.org/licenses/by/4.0/).

1. Introduction

Mine-tailings disasters represent one of the most significant environmental and humanitarian challenges associated with the mining industry [1–3]. Tailings, the waste materials produced from ore processing, contain a mixture of finely ground rock, water, and residual amounts of chemicals used in the extraction process. When containment structures fail or are overwhelmed by natural or anthropic forces, huge amounts of these tailings can be released, causing severe environmental contamination and posing serious risks to human health and livelihoods [2,4–6].

The complexity and scale of mine-tailings disasters present daunting challenges for emergency responders, environmental regulators, and affected communities alike. Effective response and recovery efforts require a deep understanding of the behaviour of tailings materials, including their transport mechanisms and dispersion patterns, as well as the potential for further environmental degradation over time. Moreover, addressing the root causes of these disasters demands comprehensive risk assessment, improved engineering practices, and robust regulatory frameworks to prevent future occurrences [7–9].

In recent years, heightened awareness of the risks associated with mine-tailings storage has spurred efforts to enhance disaster preparedness and mitigate the impacts of potential spills. Advances in technology and modelling tools have enabled increasingly accurate predictions of tailings behaviour and the development of strategies to minimize risks to

both human populations and the environment [10]. In response to the increasing awareness of these risks, there has been a growing interest in the development of numerical tools to predict the propagation and dispersion of mine-tailings spills. Thus, mine-tailings spill propagation modelling is a crucial component of assessing and mitigating the environmental impact of mining activities [11].

These models aim to simulate the movement of tailings from the source of the spill and subsequently through the environment, considering factors such as topography, hydraulics, sediment transport, and the physical and chemical characteristics of the tailings materials. One of the key challenges in mine-tailings spill propagation modelling is accurately representing the complex behaviour of the fluid once released into the environment. The rheological properties of tailings, commonly assimilated to non-Newtonian flows, can vary widely, depending on factors such as particle size distribution, mineralogy, and water content [12–14]. Additionally, the terrain over which the spill travels can greatly influence its behaviour, with steep slopes, channels, and vegetation all affecting the flow dynamics [15–18].

The simulation of the dynamics of non–Newtonian flows, such as mine tailings, can be performed by means of numerical modelling tools that are based on the solution of mass and momentum conservation equations [19–22]. To that end, the shear stress terms might be particularised by a rheological model that accounts for the properties of the fluid [19,23–25]. Additional numerical treatments might be accomplished with the aim of accurately reproducing both the dynamic and the static behaviour of the fluid over steep slopes and irregular geometries [16,26–31].

The purpose of the research presented here is the evaluation of the new features of Iber, a freely distributed depth-averaged two-dimensional hydrodynamic numerical tool (www.iberaula.com (accessed on 15 June 2024)), recently extended for modelling of non–Newtonian shallow flows. The code integrates several rheological models to consider different flow behaviours and a specific numerical scheme that determines the stopping of the fluid according to the rheological properties. The accuracy and efficiency of the simulations realised according to the implemented methods are carefully assessed in benchmarks and real case studies, showing a good agreement with the observations and the absence of numerical instabilities.

2. Materials and Methods

2.1. Numerical Simulation Tool: IberNNF

Physically-based numerical tools for the simulation of non–Newtonian flows utilise mass and momentum balance equations implemented for shallow flow conditions [16,18,32–36]. These equations, when applied to water, are known as shallow water equations (SWE). They are derived from the Navier–Stokes equations through a temporal averaging to filter out turbulent fluctuations (Reynolds Averaged Navier–Stokes, or RANS), and a depth averaging to convert the three-dimensional equations into two-dimensional ones [30,37].

The SWE, applied in a two-dimensional domain (2D-SWE), form a hyperbolic nonlinear system of three partial differential equations: one corresponding to mass conservation and the other two to momentum conservation in the x and y directions of space:

$$\frac{\partial h}{\partial t} + \frac{\partial q_x}{\partial x} + \frac{\partial q_y}{\partial y} = 0 \tag{1}$$

$$\frac{\partial q_x}{\partial t} + \frac{\partial}{\partial x}\left(\frac{q_x^2}{h} + g\frac{h^2}{2}\right) + \frac{\partial}{\partial y}\left(\frac{q_x q_y}{h}\right) = ghS_{o,x} - \frac{\tau_x}{\rho} \tag{2}$$

$$\frac{\partial q_x}{\partial t} + \frac{\partial}{\partial x}\left(\frac{q_x q_y}{h}\right) + \frac{\partial}{\partial y}\left(\frac{q_y^2}{h} + g\frac{h^2}{2}\right) = ghS_{o,y} - \frac{\tau_y}{\rho} \tag{3}$$

where h is the flow depth, q_x and q_y are the two components of depth-averaged specific discharge, g is the projected acceleration due to gravity, $S_{o,x}$ and $S_{o,y}$ are the components of the bottom slope, and τ_x and τ_y are the two components of the shear stress associated with the rheological model.

Once discretised on a computational mesh composed by elements, the first equation of the previous system shows the variation of the flow depth over time ($\partial h/\partial t$) in an element due to volume inflows and outflows ($\partial q_x/\partial x$, $\partial q_y/\partial y$) through its boundaries. The second and third equations correspond to the variations of the discharges ($\partial q_x/\partial t$, $\partial q_y/\partial t$) as functions of the forces acting on the fluids. Four terms can be distinguished (only shown for the x-component): inertia $\partial\left(q_x^2/h\right)/\partial x$ and $\partial\left(q_x q_y/h\right)/\partial y$, pressure $\partial\left(gh^2/2\right)/\partial x$, gravity through the bottom slope ($S_{0,x}$), and shear stress (τ_x).

Iber is a freely distributed, two-dimensional, depth-averaged hydrodynamic tool [38,39] currently able to simulate different environmental shallow-water flows and transport processes [16,40–52]. The previous systems of equations are solved through the Roe scheme [53], a first-order Godunov-type upwind scheme for convective fluxes and the geometric slope source term.

Iber has been recently enhanced to simulate non–Newtonian flows (IberNNF), such as dense snow avalanches [15,16]. To that end, a single-phase fluid and the shear stress grouping proposed by Julien and León [23] are assumed, besides the utilisation of an ad-hoc numerical scheme that ensures the balance among the different terms of SWE [16]. Thus, the rheological model of any particular fluid can be integrated through the shear stresses term as the addition of five components: the dispersive contribution (τ_d), the turbulent contribution (τ_t), the viscous contribution (τ_v), the Mohr–Coulomb contribution (τ_{mc}), and the cohesive contribution (τ_c).

In this work, with the aim of characterizing the static and dynamic behaviour of non–Newtonian shallow flows such as those found in mine-tailings spill propagation, two friction models have been implemented in the code. The following rheological models are expressed as friction slope (S_f), being $\tau = \rho g h S_f$.

Since the proposal of the Bingham rheological model [54], several approaches have been introduced to deal with the difficulties associated with directly obtaining the shear stress proportional to the flow velocity [55]. Some authors [56,57], assuming an incompressible and homogeneous flow, derived the following expression for the viscous (τ_v) and the Mohr–Coulomb (τ_{mc}) contributions:

$$S_f = \frac{1}{\rho g h}\left(\frac{3}{2}\tau_y + 3\frac{\mu_B v}{h}\right) \tag{4}$$

where τ_y is the yield stress, ρ is the fluid density, h is the flow depth, μ_B is the fluid viscosity, v is the flow velocity, and g is the gravitational acceleration.

Voellmy [58] presented a rheological model that considers the turbulent friction (τ_t) and the Mohr–Coulomb (τ_{mc}) terms as follows:

$$S_f = \mu + \frac{v^2}{\xi h} \tag{5}$$

where ξ is the turbulent friction coefficient, and μ is the Coulomb friction coefficient.

2.2. Test Cases

Different test cases were utilised to analyse the performance of this new extension of the numerical tool Iber for the simulation of non–Newtonian shallow flows, particularly with reference to mine-tailings propagation. The fluid was characterised by selecting a particular rheological model (Voellmy or simplified Bingham) that can represent its behaviour during the dynamic and static phases.

The first test case, originally presented by Bryant [59], consists of an idealised dam-break problem for viscous–plastic fluids that attempts to represent the release of a stored

fluid and the subsequent propagation process. The experiment defines an initial fluid height of 30.5 m and length of 305 m which is immediately released over a flat terrain. Hungr [20] presented, on the bases of this experiment, an analytical solution for a plastic fluid (ρ = 1835 kg/m^3 and total steady-state shear strength of 2390 Pa), a particular case of a simplified Bingham rheological model, and the numerical results obtained with the 1D numerical tool DAN. This experiment attempts to explore the capability of a fluid to stop and rest, given a non-horizontal free surface, such may occur with mud flows, debris flows, etc.

The second test case consists of a constant inclined plane (0.23 m/m) with a non–horizontal initial flow surface, aiming to represent the release and stop of a pyroclastic avalanche, a particular non–Newtonian flow that can be triggered by rainfall after a volcanic eruption. A detailed description of the numerical test can be found in de' Michieli Vitturi et al. [60], who simulated the avalanche dynamics with the Voellmy rheological model (μ = 0.3 and ξ = 300 m/s^2). According to the rheological properties, the fluid should stop on the inclined terrain surface. This test extends the previous one to the context of steep slopes, in which non–Newtonian unconfined flows can stop in the presence of a non–horizontal surface.

The third test case is the mine-tailings propagation caused by the failure of a gypsum pond which occurred in 1966, in East Texas (USA). Jeyapalan et al. [61] revisited the hydraulics of the pond failure, reporting the relevant observed data: the fluid was spread asymmetrically, and inside the impoundment the fluid was mobilized to points around 110 m perpendicular to the dyke and 140 m parallel to the dyke. This caused the mobilisation of around of 80,000–130,000 m^3 of gypsum tailings, which flowed some 300 m beyond the dyke in 60–120 s. From a previous analysis, the fluid was characterized as Bingham type with a flow density of 1400 kg/m^3, a yield stress of 1000 Pa, and a viscosity of 50 Pa·s.

Finally, the mine-tailing pond failure of Los Frailes (Aznalcóllar, Spain), which occurred on 25 April 1998, was utilised to test the numerical tool under real conditions. When the failure occurred, after a very fast breach formation that affected the two lagoons [62–64], the stored fluids (pyroclastic and pyritic tailings) were spilled and probably mixed. Their properties changed during the spill [65], and thus, the flow probably propagated as a unique hyper-concentrated fluid [66,67]. Despite the uncertainties in the hydraulics of the event [66], the fluid was assumed to behave as a Bingham plastic, with the aim of testing the performance of the numerical tool for simulating non–Newtonian shallow flows. Additionally, the spilled hydrograph proposed by Consultec Ingenieros [68] was used as inflow at the breakpoint. A bulk density of 3100 kg/m^3 was assumed, being the parameters of the rheological varied from 0 to 50 Pa for the yield stress (τ_y) and from 0 to 2000 Pa·s for the fluid viscosity (μ_B). The test was oriented as a sensitivity analysis instead of as a reconstruction of the flood event (Table 1).

Table 1. Summary of the simulated scenarios in the studied case of the mine-tailing pond failure of Los Frailes.

Parameter	Range	Increments
Yield stress, τ_y [Pa]	0–50	5
Viscosity, μ_B [Pa·s]	0–2000	5

3. Results

3.1. Idealised Dam-Break Problem for Viscous–Plastic Fluids

The calculation domain of 2000 m length was discretized with one-dimensional elements of 1 m length. According to Hungr [20], the rheological model selected was the simplified Bingham, but one only considering a total yield stress contribution of 2390 Pa (i.e., $\rho g h S_f$ = 2390 Pa). Results were compared with an approximated energy solution

presented in Hungr [20], with a runout distance of 1896 m, and those of a DAN model, a one-dimensional numerical model developed ad hoc by the same author.

Figure 1a (green line) shows the fluid profile at the end of the simulation, which stopped at 130 s with a runout distance of 1875 m. The results show a good agreement with the detention time and runout distance of the analytical solution (Figure 1a, red line), in addition to the results of the DAN model (Figure 1a, blue dots). A non-horizontal free surface was obtained with the fluid at rest.

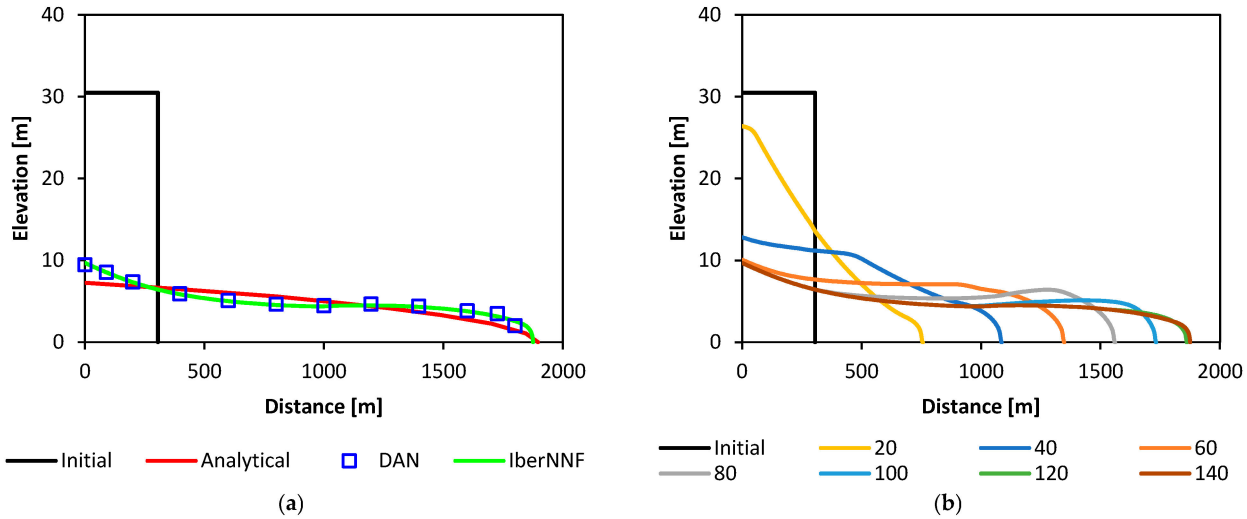


Figure 1. Dam-break of an idealised mine-tailings dam. (**a**) Final runout profile of the presented code (green line), compared to the analytical solution (red line) and the numerical solution of the DAN model (blue dots), as presented by Hungr [20]. (**b**) Runout profile evolution obtained with the presently described code, for each 20 s.

The evolution of the simulated fluid profile is plotted in Figure 1b for each 20 s, showing the particular behaviour of the fluid according to the rheological model used. This results in a non–horizontal final shape with fluid depths at the leading-edge higher than intermediate positions during the dynamic phase. The resulting wave-front velocities were 22.6, 16.5, 13.1, 10.6, 8.6, 6.5, and 1.4 m/s respectively, decreasing gradually.

This test shows the good performance of the presented numerical model, especially in those configurations where non-velocity terms of the rheological model are neglected. Hence, the fluid stops according to the yield stress contribution, which depends on the flow depth at each location and time step.

3.2. Fluid Detention on Sloping Terrain

A particular test over steep slopes is presented by de' Michieli Vitturi et al. [60], aiming to show the performance of IMEX_SfloW2D, a numerical tool developed to simulate pyroclastic avalanches in volcanic regions. A non-stable condition for an initial fluid over an inclined plane was imposed and then immediately released. Such initial condition was implemented by raster data, being the fluid-rheology Voellmy type. The domain was discretised with one-dimensional elements of 1 m in length.

Figure 2 compares the results of both numerical models. Circles correspond to IMEX_SfloW2D, while coloured lines represent the results obtained with the presented numerical model. In both cases the fluid stopped over the inclined plane, showing a quite similar solution. Since the free surface of the left side of the initial volume has a slope less than the Coulomb friction coefficient (μ), the avalanche did not move upstream; otherwise, the avalanche should move to reach an equilibrium state according to the fluid characteristics.

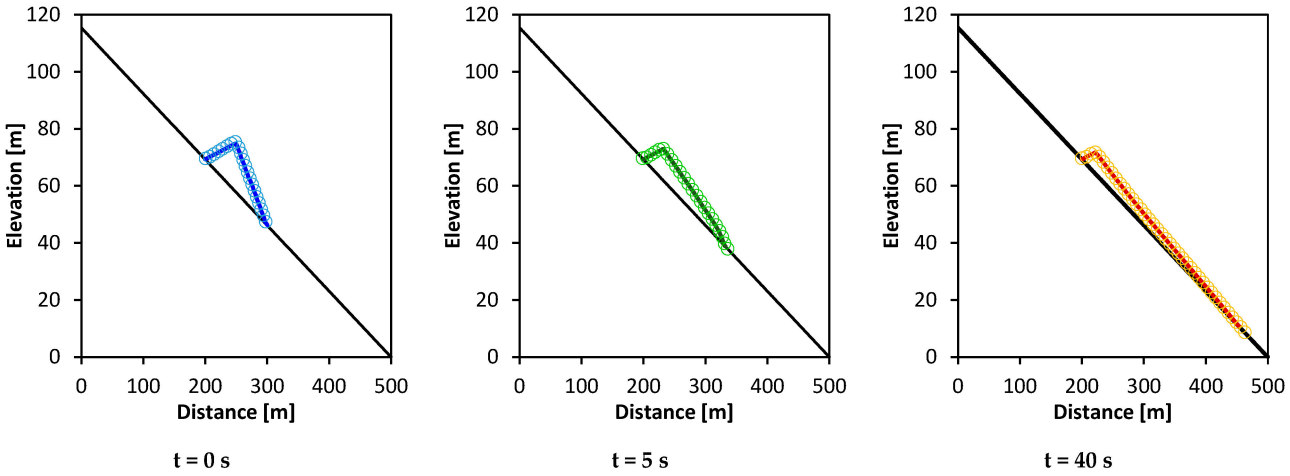


Figure 2. Idealised test case of a pyroclastic avalanche proposed by de' Michieli Vitturi et al. [60]. Numerical results for a Voellmy-like fluid with $\mu = 0.3$ and $\xi = 300$ m/s^2: original data (circles) and simulated results (lines). The black line represents the topography.

3.3. Idealised Gypsum Spill (East Texas, USA)

The impoundment dimensions of the gypsum pond presented by Jeyapalan et al. [61] were idealized to 280 m in length and 110 m in width, with the breach spanning 120 m in width and 20 m in thickness. The initial condition was assumed to be a constant height of 11 m, and the fluid was released instantaneously. The computational domain, spanning 510 m in length and 400 m in width, was discretized into triangular-shaped elements of 2 m mean side length. The total number of elements was 105,936. The fluid was assumed to be Bingham type ($\tau_y = 1000$ Pa and $\mu_B = 50$ Pa·s).

Figure 3 depicts the spill propagation each 30 s. The fluid spread asymmetrically due to the idealised geometry of the impoundment. The maximum simulated runout was 265 m, the wave front being stopped at 50 s, while the detention of the fluid was completely produced at 102 s. The spread volume from the impoundment was 170,620 m^3, while the remainder was 176,804 m^3, with a maximum height of 7 m.

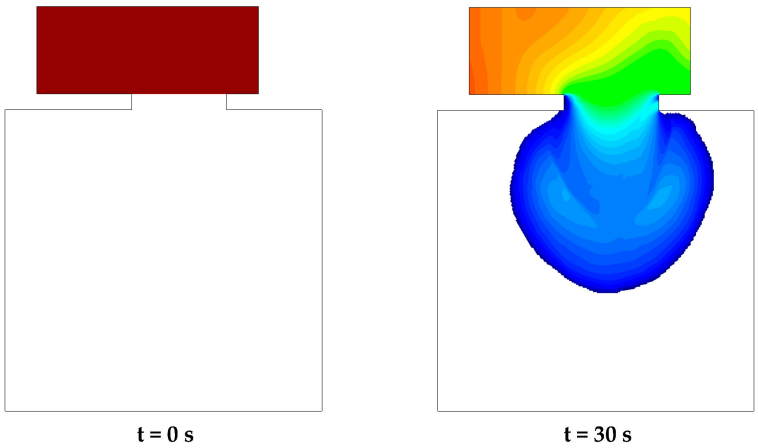


Figure 3. *Cont.*

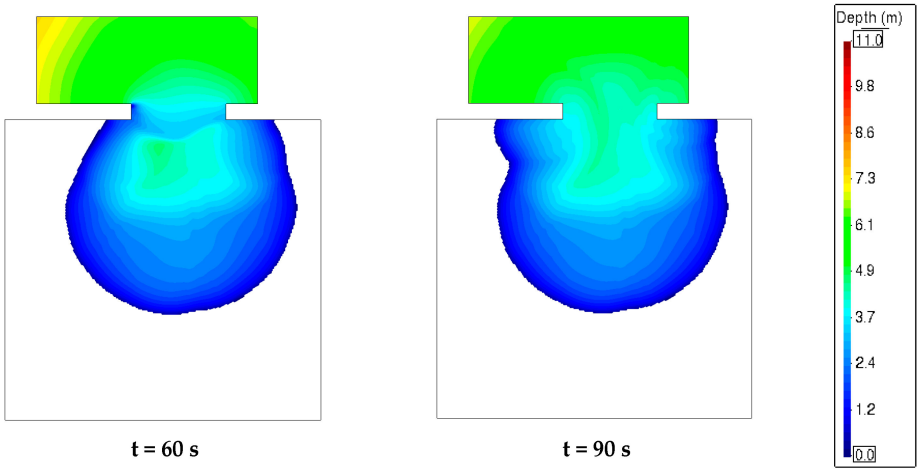


Figure 3. Results of the simulation considering a Bingham-like fluid in an idealised geometry of the gypsum pond failure that occurred in 1966 in East Texas (USA). Depth evolution each 30 s.

3.4. Pond Failure of Los Frailes (Spain)

The simulation of the spill was limited to the upper part of the more than 85 km of the total observed flood, extending from the point of failure (Figure 4a, red star) to El Guijo gauge station (Figure 4a, blue circle), located 7.1 km downstream of that point. The modelled area spans approximately 1000 ha over a distance of 9 km and encompasses a predominantly flat terrain comprising alluvial terraces, including the convergence point of the Guadiamar and Agrio rivers (Figure 4a). An unstructured mesh composed of triangular elements with a mean side length of 10 m was utilised to discretise the calculation domain, generating 219,330 elements (Figure 4b).

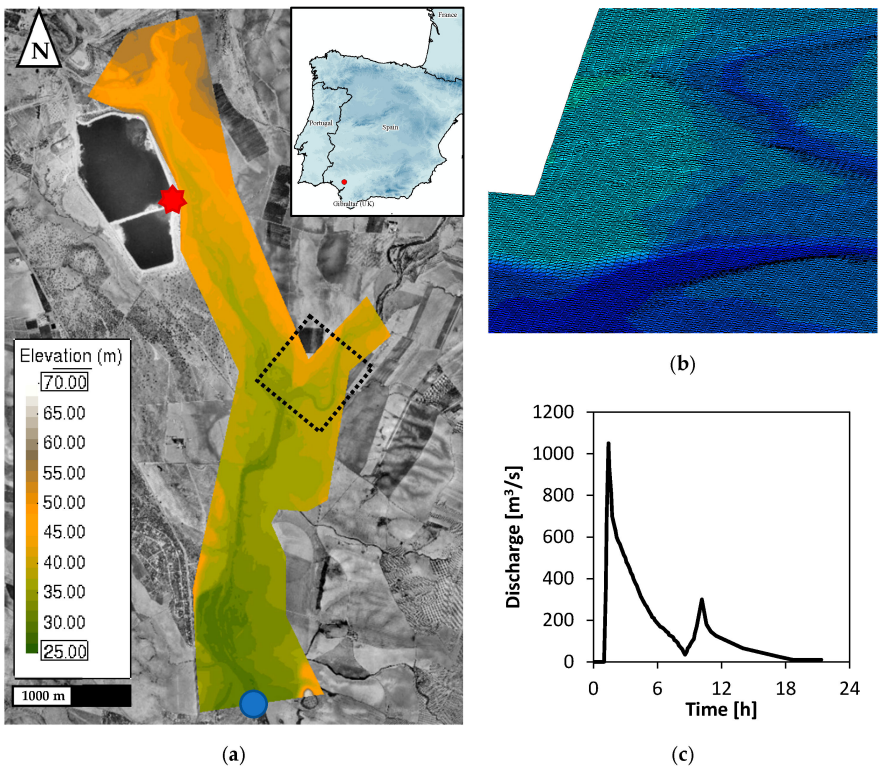
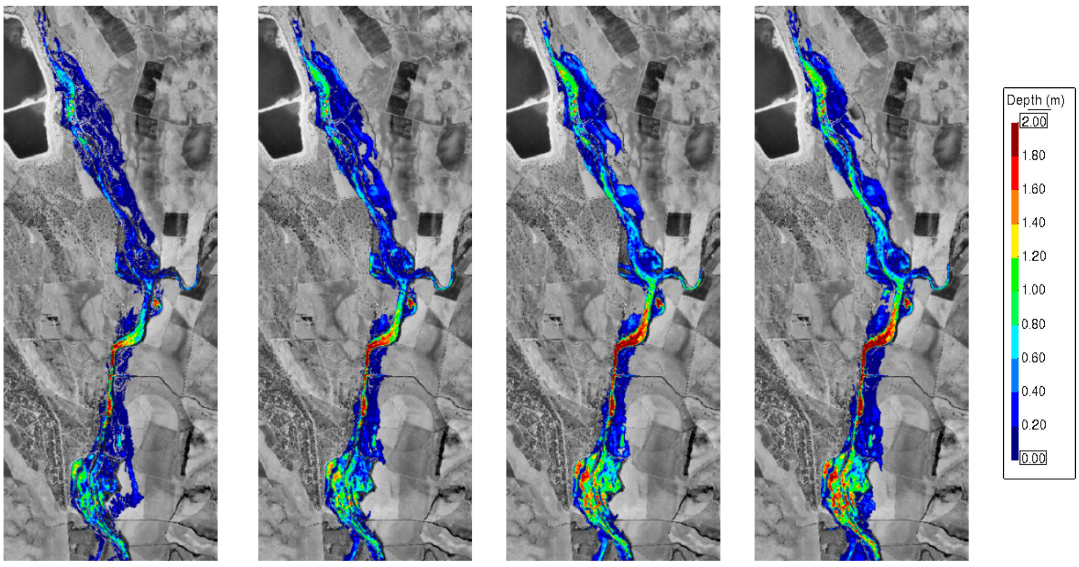


Figure 4. (**a**) General location of the Los Frailes mine pit, topography of the terrain, breakpoint (red star) and gauge station (blue circle). (**b**) Mesh discretisation at the Agrio River and Guadiamar River junction (dotted rectangle in (**a**)). (**c**) Estimated hydrograph generated after the pond break.

Post-failure topographical data, consisting of a Digital Terrain Model (DTM) with a 5 × 5 m pixel size, were utilized to update the elevations of the nodes due to the unavailability of an original dataset acquired previous to the event. It is worth noticing that modifications to the riverbed and banks occurred subsequent to the spill event as part of river restoration efforts [69–71], potentially leading to differences in the topographical features.

The simulation process involved varying the Bingham parameters to analyse the performance of the numerical model. The parameters τ_y and μ_B were systematically varied within ranges of 0 to 50 Pa and 0 to 2000 Pa·s (see Table 1). An initial analysis was made with the aim of understanding the flow behaviour by independently varying the yield stress and Bingham viscosity parameters. Subsequently, a combination of both parameters was tested together.The inlet boundary condition was defined by the hydrograph (Figure 4c) of the spill originated at the junction of the two lagoons, as represented by the red star in Figure 4a. This hydrograph was derived through an iterative process of inverse convolution from the recorded data at the gauge station [68]. This process was first carried out by means of the numerical tool HEC-1, and then with the numerical tool HEC-RAS to obtain the discharge–volume relations, and, finally, the "Modified Puls" routing method was used to obtain the hydrograph at the breaking point. A critical flow regime was imposed as an outlet condition at the El Guijo gauge station.

In the first analysis, the yield stress was again revealed to have a significant role in fluid retention. As expected, an increase in τ_y resulted in a higher volume of retained spill. Figure 5 illustrates this effect, showing that for low values of τ_y, the flow extension increases near the discharge point, but with smaller flow depths (Figure 5a). Conversely, higher τ_y values lead to a smaller extension near the breakpoint, but greater extension downstream, with higher flow depths observed in both areas (Figure 5d).



(**a**) (**b**) (**c**) (**d**)

Figure 5. Retained flow at the end of the simulation, considering null viscosity (μ_B = 0 Pa·s) and different values of the yield stress: (**a**) τ_y = 5 Pa; (**b**) τ_y = 15 Pa; (**c**) τ_y = 25 Pa; and (**d**) τ_y = 50 Pa.

On the other hand, Bingham viscosity affects flow behaviour in terms of flow propagation velocity, albeit without retention capacity, exhibiting a Manning-like behaviour in water flows. Figure 6a illustrates simulated hydrographs at the outlet boundary for various values of μ_B (25, 50, 200, 1000, 1500, and 2000 Pa·s), with τ_y = 0 Pa. An attenuation of the hydrograph is observed as Bingham viscosity increases, with the second peak becoming almost negligible for values greater than 200 Pa·s. For μ_B values less than 50 Pa·s, the simulated results closely match the observed ones (Figure 6a). The arrival time of the

flood at the gauge station is well-captured for μ_B = 25 Pa·s, although there is a slight underestimation of the peak discharge. The numerical model also reproduces the second peak well for low values of μ_B.

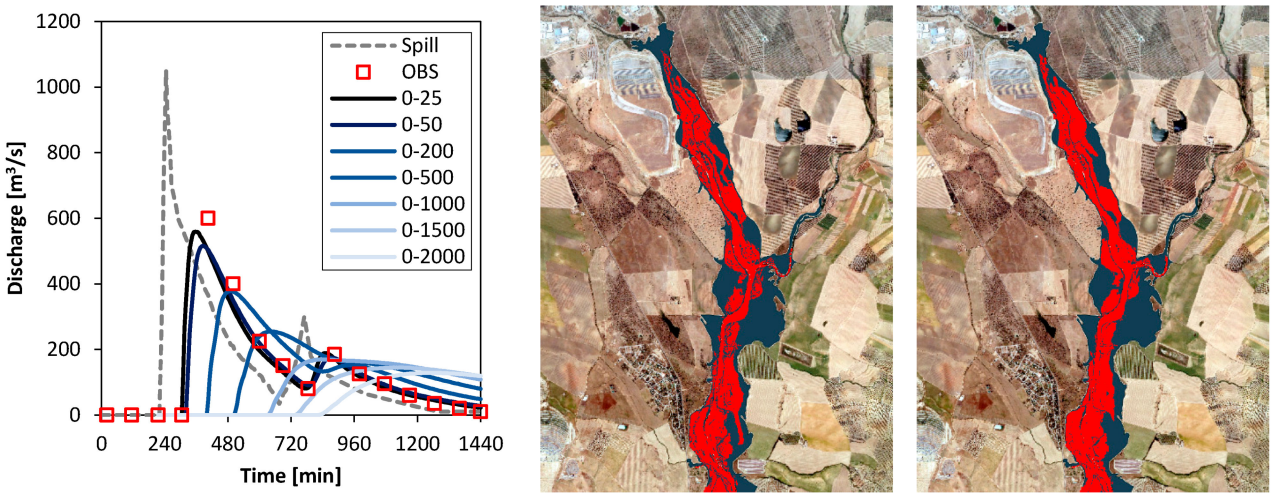


Figure 6. (**a**) Estimated hydrograph (red squares) and results of the different μ_B values tested (purple lines). Simulated flood extension (red polygon) and observed flood recorded by Landsat TM on 30 April: (**b**) τ_y = 25 Pa and μ_B = 5 Pa·s; (**c**) τ_y = 25 Pa and μ_B = 15 Pa·s.

Figure 6b,c illustrate the best-fit result of combining τ_y and μ_B values considering the previous analysis. The simulated flood extension is compared with the satellite image taken in the study area five days after the disaster, on 30 April (dark-blue polygon), which was then used to define amendments in contaminated soils [13]. These figures show the extension of the computed flood (red polygon) overlaid on the registered flood (dark-blue polygon) for two different combinations of the Bingham parameters: τ_y = 25 Pa and μ_B = 5 Pa·s (Figure 6b); and τ_y = 25 Pa and μ_B = 15 Pa·s (Figure 6c).

Despite both parameter combinations having the same τ_y value, significant differences in flood extension are observed due to the reduction of velocity for μ_B = 15 Pa. When the velocity is low because the resistance forces are high, there is greater retention of the flood. This effect is particularly noticeable downstream of the river's junction, where a more continuous extension of the computed flood is observed.

4. Discussion

4.1. On the Numerical Approach

In general, in the numerical modelling of non–Newtonian fluids using 2D shallow-water equation (2D-SWE)-based models, the flow is simulated as a continuum. In this approach, the individual movement of particles that could occur in nature cannot be simulated. However, most fluidified mine tailings behave as a continuum, and simulation tools based on 2D-SWE can be used here to describe their dynamics as long as the different terms of 2D-SWE are well balanced [16,27,72]. Nevertheless, the intrinsic assumptions for obtaining the system of 2D-SWE, together with the uncertainty/variability in field observations [73], may lead to uncertainties in the flood extent and in the internal movements of the particles, but this occurs for all numerical models, since they are simplifications of reality.

In numerical flow modelling, it is necessary to establish a wet–dry depth limit for an accurate characterization of wave fronts while preserving mass, which is a threshold used to consider whether there is flow in a mesh element or not. This is a relevant parameter for water flow, especially for flooding in flat areas [74–76], and for hydrological processes modelling [40,47,77], but it also applies to non–Newtonian fluids such as those occurring in mine-tailings spill propagation modelling. Very large wet–dry limits, greater than a few cen-

timetres, can significantly alter flow propagation, especially as to the flow front [38,40]. The wet–dry limit must be properly defined, considering, in general, the geometric dimension of the problem, mesh size, expected flow depth, and, particularly, fluid properties. Additionally, selecting the appropriate numerical scheme to handle wet–dry fronts, especially the drying method, is crucial for preserving mass conservation [28,29,31,53].

There are few references on wet–dry limit treatment for non–Newtonian shallow flow models based on the solution of the 2D-SWE. For this type of flow, the individual and/or aggregate particle size is generally smaller than a few millimetres; since the fluid is simulated as a continuum, wet–dry limit values from 0.001 to 0.01 m can be sufficient to properly define the dynamics and extent of the flood. A value of 0.01 m was chosen for all simulations, but further investigation is necessary to fully understand the role of this parameter in the simulation of non–Newtonian shallow flows.

4.2. On the Rheological Models

Rheological models to describe both the dynamic and static phase of non–Newtonian shallow flows exist for a wide field of applications. In particular, in contexts related to environmental flows, and, especially, shallow flows, several rheological models have been developed to describe the relationship between the shear stress and the shear rate [78].

From the simplest potential law to the full—and complex—Bingham model, several rheological models exist in the literature, the development of each one being oriented to achieve a particular reproduction of a fluid behaviour. The aim of the present work is not to test as many rheological models as possible—or all that exist. Although this would allow a broader simulation of the behaviour of non-Newtonian shallow fluids, some rheological models are not appropriate to fluids that have a non–horizontal free surface at rest.

Rheological models that only integrate velocity-dependent terms do not allow the detention of the fluid, such as occurs with water flows in unconfined geometries. This would be the case of Manning-based rheological models.

The Manning rheological model, an empirical equation widely utilised in hydraulics and hydrology, applies to uniform flow in open channels and is a function of the channel velocity, flow area, and channel slope:

$$S_f = \frac{n^2 v^2}{h^{4/3}} \tag{6}$$

where n is the Manning coefficient, v is the flow velocity, and h is the flow depth. It is related to turbulent friction (τ_t), which is utilised by several authors in simulating hyperconcentrated flows [79–82]. The unique value for calibration is the Manning coefficient (n).

In work similar to the Manning rheological model, while considering constant sediment concentration and uniform flow, Macedonio and Pareschi [83] proposed the following relation of the shear stress: $\tau = \tau_y + \mu_1 (dv/dz)^{\alpha}$, where τ_y is the yield stress, μ_1 is a proportionality coefficient, and α is the flow behaviour index.

When α = 2, a dilatant flow behaviour is expected:

$$S_f = \frac{n^2 v^2}{h^3} \tag{7}$$

The same authors also presented the application of the Manning equation to viscous flows by particularizing the parameter α = 1. This allows for the representation of viscous flows:

$$S_f = \frac{n^2 v}{h^2} \tag{8}$$

A similar behaviour is expected in those models that also integrate non–velocity-dependent terms, such as the Voellmy and simplified Bingham, when the velocity-dependent terms are neglected. O'Brien [84] derived an expression for the representation of

the shear stress of mudflows, being a quadratic equation that integrates the Mohr–Coulomb term, the viscous term, and the turbulent term as follows:

$$S_f = \frac{\tau_y}{\rho g h} + \frac{K \mu_B v}{8 \rho g h^2} + \frac{n^2 v^2}{h^{4/3}} \quad (9)$$

where τ_y is the yield stress, ρ is the fluid density, g is the gravitational acceleration, h is the flow depth, K is a resistance parameter, μ_B is the flow viscosity, v is the flow velocity, and n is the Manning coefficient. With this approach, the fluid continues flowing when the yield stress contribution is omitted.

Bartelt et al. [85] developed a resistance term related to the cohesion, a physical property of the fluid. This rheological model is non–velocity-dependent and is expressed as follows:

$$S_f = \frac{1}{\rho g h} \left(C_B \left(1 - \mu\right) \left(1 - e^{-\frac{\rho g h}{C_B}} \right) \right) \quad (10)$$

where ρ is the fluid density, g is the gravitational acceleration, h is the flow depth, C_B is the cohesion, and μ is the Coulomb friction coefficient. Although this model is functional and allows for the stopping of the fluid within unconfined and irregular slopes, it is commonly used together with the Voellmy model.

4.3. On the Performance of Iber in Simulating Mine-Tailings Spill Propagation

The test case of a sloping terrain presented in de' Michieli Vitturi et al. [60] was originally developed for the simulation of pyroclastic avalanches, such as those produced in post-eruptive events in volcano regions. However, some mining activities generate similar materials, which, in contact with water, have similar behaviours when released after the break of a mine pond [62,63,66,86–92]. Apart from the particularities of the test, the extension of Iber for simulating non–Newtonian shallow flows was proved to be valid, even for steep slopes. The fluid can stop on steep terrains thanks to the specific numerical scheme utilised in which non–velocity-dependent terms of the rheological model are used to counterbalance the pressure forces [16]. This can be useful in several situations, such as for mine ponds located in mountain regions [2,93,94]. The use of a well-balanced numerical scheme avoids oscillations leading to numerical instabilities; otherwise, the imbalance can make them incapable of simulating even quiescent states over both simple and complex geometries [27–31,95,96].

The simulation of a gypsum spill caused by the failure of a pond in East Texas in 1966 [61] was utilised to show the performance of the numerical model over two-dimensional domains. Some differences were observed due to important assumptions and simplifications applied not only in the domain discretisation, but also in the topographical data. The simulated runout distance was smaller than the reported one, which might have been caused by the assumption of a completely horizontal flat terrain and, particularly, the rheological model utilised. But other factors should not be discarded.

In this regard, the yield stress term in Equation (4) is multiplied by a factor of 1.5; this means the contribution of a 50% higher yield stress term than found in similar numerical models that use a Bingham-based rheological model without this factor [84,97,98].

Aiming to show the influence of this factor in the simulations, the same case was re-calculated, omitting this factor, which showed a better performance in term of runout. Figure 7 compares the flow behaviour considering the increased factor of 1.5 in the yield stress terms (upper row), according to the proposal of [56,57], and without considering this factor (lower row). In this last case, the runout distance reached 300 m, in agreement with the observations [61]. Despite the differences in the resistance terms, the leading edge of fluid stopped at 50 s in both cases, keeping a similar shape as to the flood extent. In this sense, in both cases the released volume was higher than the estimations, but was within the same order of magnitude as the values presented by Jeyapalan et al. [61]. Despite the fact that the freezing time agrees with the observations, the uncertainties in the breach formation (breaking time and shape evolution of the breach) and the possible fluidification

of the stored fluid [65] might favour a lack of representation of the fluid behaviour during the dynamic and static phase [66].

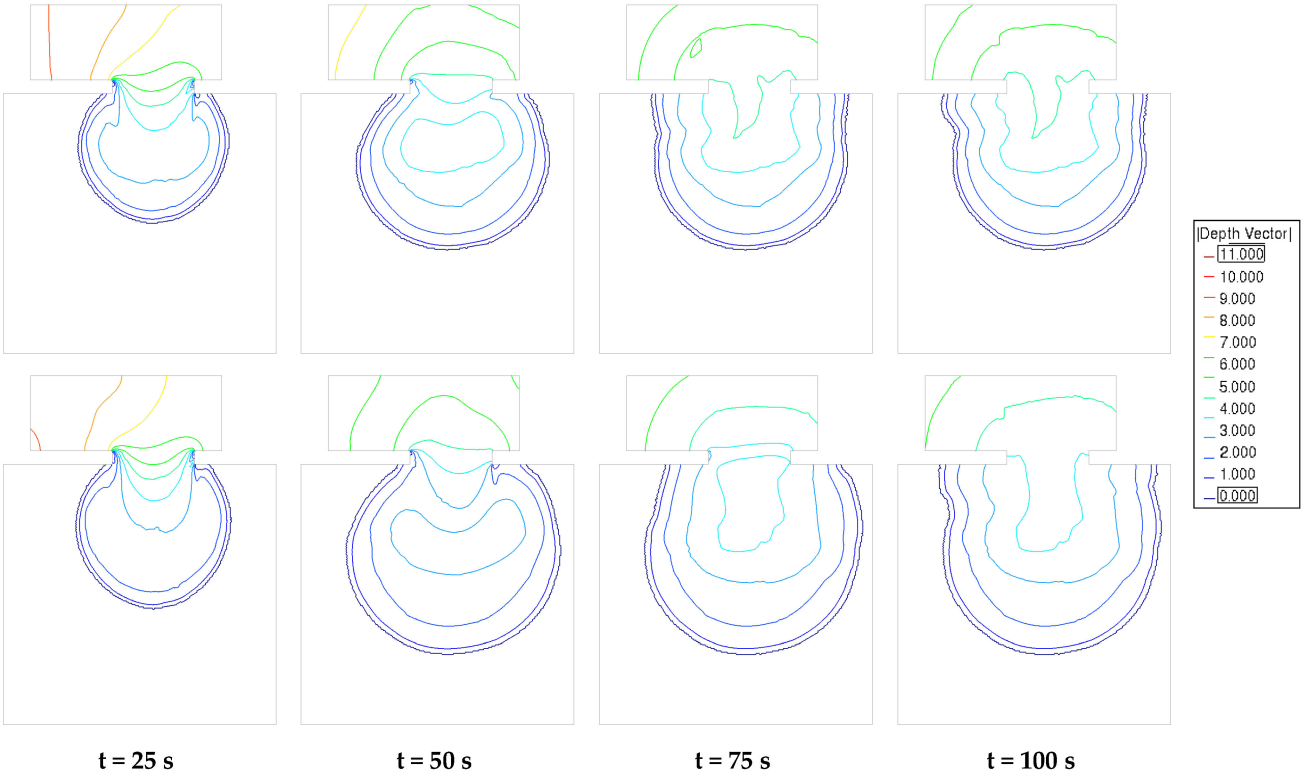


Figure 7. Idealised gypsum spill. Contour line depth evolution when using the simplified Bingham rheological model with an increased factor of 1.5 in the yield stress, according to [56,57] (**upper row**), and without the increased factor in the yield stress term (**lower row**).

Finally, despite the fact that the Los Frailes mine pond failure was not utilised to reproduce the event, the presented results highlight some discrepancies with the observations. The topographical data utilized was the most recent Digital Terrain Model (DTM) provided by the Instituto Geográfico Nacional. However, significant morphological changes occurred after the accident due to the removal operations of the deposited muds, and the river restoration program known as "El Corredor Verde del Guadiamar" [70].

Data recorded at El Guijo gauge station suggested the presence of two peaks, but its poor quality necessitated an ad hoc hydraulic study to reconstruct the spill's hydrograph [66]. Nevertheless, this hydrograph was then utilized as an inlet condition at the failure point, potentially generating differences in the spill reconstruction. A portion of the spilled fluid, predominantly composed of pyrite, remained and ceased flowing, indicating a mudflow-like behaviour. A Bingham-type fluid was assumed, but a hyper-concentrated behaviour (sediment-laden flow) cannot be discarded, given the observations made during the spill [66,67]. In any case, the performance of the extension of Iber to simulate real scenarios of non–Newtonian shallow flows, such as mine-tailing spills, was proved to be suitable.

4.4. On the Code Optimization and Computing Time for GPU-Computing

Iber is a numerical tool explicit in time; hence, the CFL stability criterion applies over the computational time step [99]. This condition establishes a relation between the water depth, the flow velocity, the wave celerity, the size of the element, and the maximum permissible computational time step. The extension of Iber for the simulation of non–Newtonian shallow flows uses the computational time step proposed by Cea and

Bladé [40], with a value of CFL = 0.45 being used in all test cases for numerical stability. Iber automatically calculates the calculation time steps for solving the equations.

Thus, high flow depths and velocities, in addition to small-sized elements, notably increase the computational time. The current version of IberNNF is CPU-based, which is partially parallelised using OpenMP. This means that, at most, only "speed-ups" corresponding to the number of CPU cores can be obtained. When dealing with the simulations of mine-tailings propagation case studies, the problem domain or/and the resolution needed to assess the fluid dynamics could notably increase the computation time.

Future work should focus on the application of general-purpose computing on graphics processing unit (GPGPU) techniques [100,101] to parallelise the code for GPU computing, such as seen in the water-based hydrodynamic, habitat, and sediment-transport modules of Iber, called R-Iber [50,102]. With that, together with a code optimization, the computing process will reach speed-ups above 100-times that of the sequential version. With the aim of testing the current applications, the model is freely distributed as a part of the software suite through www.iberaula.com (accessed on 15 June 2024).

4.5. On the Associated Risk of Mining Activities

Mining activities, while essential for the extraction of valuable minerals and resources, pose several associated risks that can impact the environment, human health, and local communities. To that end, guidelines for the design, construction, monitoring, and closure of tailings dams are mandatory to manage and prevent hazardous situations. Following these recommendations can greatly reduce the risks of failures and dangerous conditions for both people and the environment [2,94].

Nevertheless, more than 150 major tailings-dam failures have been reported since 1961, with a wide variety of materials being released [93]. This means 2.5 failures per year, on average, 82 of them having occurred in the 2000–2024 period. This reveals a clear necessity for additional—and in-depth—management, monitoring, prevention, and planning strategies to reduce the associated flood risks of mining activities [2,103].

The development of numerical simulation tools can help in addressing several engineering problems related to mining activities and can also help in reducing the risk of a failure and the subsequent occurrence of situations dangerous for people and the environment, due to the release and propagation of uncontrolled spills. Understanding the characteristics of tailings ponds, including their construction and filling processes, as well as the type of fluid stored (and whether it maintains Newtonian properties), is essential [66] for properly addressing not only the reconstruction of a past event but also the evaluation of the risk of future failure or malfunction scenarios in mine-tailings dams that might cause flood events.

5. Conclusions

Numerical modelling of non–Newtonian fluids using 2D shallow water equations (2D-SWE) simulates the flow as a continuum. Despite the fact that it might not capture individual particle movements accurately, this approach is quite useful for the simulation of the propagation of a mine-tailings spill after a dam failure.

To that end, specific rheological models are used to describe both static and dynamic behaviours. However, not all rheological models are suitable for fluids with non–horizontal free surfaces at rest. Only those that contain non–velocity-dependent terms, such as Bingham or Voellmy models, among others, can retain the flow in unconfined geometries and step slopes.

This work presents the extension of the hydraulic numerical tool Iber for the simulation of non–Newtonian flows, in particular, mine tailings. This extension draws on the developments carried out for the simulation of snow avalanches, but the friction terms have been particularized to rheological models capable of representing the dynamic and static behaviours in the propagation of mine tailings.

The different case studies utilised to test the code proved that the numerical tool is capable of simulating this type of fluid under different situations, such as the obtaining of a non–horizontal free surface for a fluid at rest, and the stopping of the fluid in an area with a slope, according to the properties of the fluid, as well as demonstrating its usefulness in real cases. The code performed suitably, providing reliable results without numerical instabilities, even when using a wet–dry limit of 0.01 m, which provided a good description of the flooded area.

The development or enhancement of numerical tools for evaluating flood hazards and risks associated with mining dam failure is crucial. These tools should not only assess the potential impact of such failures, but also propose effective mitigation measures and contribute to the development of guidelines for constructing safer structures. These tools must accurately predict the extent and severity of flooding that could result from a mining dam failure. They should provide insights into vulnerable areas and describe potential damage to infrastructure and communities and the likelihood of loss of life. By doing so, they enable stakeholders to make informed decisions about emergency response planning, evacuation routes, and the implementation of protective measures, in addition to contributing to the development of guidelines for constructing safer mining structures in the future.

Author Contributions: Conceptualization, M.S.-R. and E.B.; methodology, M.S.-R., M.S.-J. and E.B.; software, M.S.-R. and E.B.; validation, M.S.-J. and T.D.; resources, M.S.-R.; data curation, M.S.-R. and E.B.; writing—original draft preparation, M.S.-R.; writing—review and editing, E.B., M.S.-J. and T.D.; supervision, E.B. All authors have read and agreed to the published version of the manuscript.

Funding: This research received no external funding.

Data Availability Statement: The data presented in this study are available on request from the corresponding author.

Acknowledgments: The authors thank Beningno Bayán, retired engineer of Confederación Hidrográfica del Guadalquivir and member of the 'Plan Doñana 2005' scientific commission, for his collaboration in helping to understand the physics of the spill, and his generous work of information-searching, particularly as to the case study 'Pond Failure of Los Frailes'.

Conflicts of Interest: The authors declare no conflict of interest.

References

1. Hudson-Edwards, K.A.; Macklin, M.G.; Jamieson, H.E.; Brewer, P.A.; Coulthard, T.J.; Howard, A.J.; Turner, J.N. The impact of tailings dam spills and clean-up operations on sediment and water quality in river systems: Rios Agrio–Guadiamar, Aznalcollar, Spain. *Appl. Geochem.* **2003**, *18*, 221–239. [CrossRef]
2. Kheirkhah Gildeh, H.; Halliday, A.; Arenas, A.; Zhang, H. Tailings Dam Breach Analysis: A Review of Methods, Practices, and Uncertainties. *Mine Water Environ.* **2021**, *40*, 128–150. [CrossRef]
3. Owen, J.R.; Kemp, D.; Lèbre, É.; Svobodova, K.; Pérez Murillo, G. Catastrophic tailings dam failures and disaster risk disclosure. *Int. J. Disaster Risk Reduct.* **2020**, *42*, 103361. [CrossRef]
4. Roche, C.; Thygesen, K.; Baker, E. *Mine Tailings Storage: Safety Is No Accident*; United Nations Environment Programme: Nairobi, Kenya; GRID-Arendal: Arendal, Norway, 2017; ISBN 978-82-7701-170-7.
5. Ngole-Jeme, V.M.; Fantke, P. Ecological and human health risks associated with abandoned gold mine tailings contaminated soil. *PLoS ONE* **2017**, *12*, e0172517. [CrossRef] [PubMed]
6. Martínez-Gomariz, E.; Barbero, C.; Sanchez-Juny, M.; Forero-Ortiz, E.; Sanz-Ramos, M. Dams or ponds classification based on a new criterion to assess potential flood damage to roads in case of failure. *Nat. Hazards* **2023**, *117*, 625–653. [CrossRef]
7. Hudson-Edwards, K.A.; Jamieson, H.E.; Lottermoser, B.G. Mine wastes: Past, present, future. *Elements* **2011**, *7*, 375–380. [CrossRef]
8. Kossoff, D.; Dubbin, W.E.; Alfredsson, M.; Edwards, S.J.; Macklin, M.G.; Hudson-Edwards, K.A. Mine tailings dams: Characteristics, failure, environmental impacts, and remediation. *Appl. Geochem.* **2014**, *51*, 229–245. [CrossRef]
9. Bowker, L.N.; Chambers, D.M. The Risk, Public Liability and Economics of Tailings Storage Facility Failures. *Earthwork Act* **2015**, *24*, 56.
10. Mudd, G.M. The Environmental sustainability of mining in Australia: Key mega-trends and looming constraints. *Resour. Policy* **2010**, *35*, 98–115. [CrossRef]
11. Dong, L.; Deng, S.; Wang, F. Some developments and new insights for environmental sustainability and disaster control of tailings dam. *J. Clean. Prod.* **2020**, *269*, 122270. [CrossRef]

12. López-Pamo, E.; Barettino, D.; Antón-Pacheco, C.; Ortiz, G.; Arránz, J.C.; Gumiel, J.C.; Martínez-Pledel, B.; Aparicio, M.; Montouto, O. The extent of the Aznalcollar pyritic sludge spill and its effects on soils. *Sci. Total Environ.* **1999**, *242*, 57–88. [CrossRef] [PubMed]
13. Madejón, P.; Domínguez, M.; Madejón, E.; Cabrera, F.; Marañón, T.; Murillo, J. Soil-plant relationships and contamination by trace elements: A review of twenty years of experimentation and monitoring after the Aznalcóllar (SW Spain) mine accident. *Sci. Total Environ.* **2018**, *625*, 50–63. [CrossRef] [PubMed]
14. Tornero, V.; Arias, A.M.; Blasco, J. Following the Aznalcóllar toxic spill. *Environ. Res.* **2011**, *111*, 1033–1036. [CrossRef] [PubMed]
15. Sanz-Ramos, M.; Andrade, C.A.; Oller, P.; Furdada, G.; Bladé, E.; Martínez-Gomariz, E. Reconstructing the Snow Avalanche of Coll de Pal 2018 (SE Pyrenees). *GeoHazards* **2021**, *2*, 196–211. [CrossRef]
16. Sanz-Ramos, M.; Bladé, E.; Oller, P.; Furdada, G. Numerical modelling of dense snow avalanches with a well-balanced scheme based on the 2D shallow water equations. *J. Glaciol.* **2023**, 1–17. [CrossRef]
17. Zugliani, D.; Rosatti, G. TRENT2D❄: An accurate numerical approach to the simulation of two-dimensional dense snow avalanches in global coordinate systems. *Cold Reg. Sci. Technol.* **2021**, *190*, 103343. [CrossRef]
18. Medina, V.; Hürlimann, M.; Bateman, A. Application of FLATModel, a 2D finite volume code, to debris flows in the northeastern part of the Iberian Peninsula. *Landslides* **2008**, *5*, 127–142. [CrossRef]
19. Xia, C.; Tian, H. A Quasi-Single-Phase Model for Debris Flows Incorporating Non–Newtonian Fluid Behavior. *Water* **2022**, *14*, 1369. [CrossRef]
20. Hungr, O. A model for the runout analysis of rapid flow slides, debris flows, and avalanches. *Can. Geotech. J.* **1995**, *32*, 610–623. [CrossRef]
21. Wu, T.; Vuong, T.; Wang, C.; Chu, C.; Lin, C. Model development for simulating mudslide and the case study of the failure of the gypsum tailings dam in East Texas in 1966. *Nat. Hazards Earth Syst. Sci. Discuss.* **2020**. *preprint*. [CrossRef]
22. Ding, W.; Wang, G.; Yang, Q.; Xu, Y.; Gao, Y.; Chen, X.; Xu, S.; Han, L.; Yang, X. Risk Assessment and Control of Geological Hazards in Towns of Complex Mountainous Areas Based on Remote Sensing and Geological Survey. *Water* **2023**, *15*, 3170. [CrossRef]
23. Julien, P.Y.; Leon, C. Mudfloods, mudflows and debris flows, classification in rheology and structural design. In Proceedings of the International Workshop on the Debris Flow Disaster, Caracas, Venezuela, 14–16 December 1999.
24. Hu, J.; Li, K.; Su, W.; Zhao, X. Numerical Simulation of Drilling Fluid Flow in Centrifugal Pumps. *Water* **2023**, *15*, 992. [CrossRef]
25. Melo, M.; Eleutério, J. Probabilistic Analysis of Floods from Tailings Dam Failures: A Method to Analyze the Impact of Rheological Parameters on the HEC-RAS Bingham and Herschel-Bulkley Models. *Water* **2023**, *15*, 2866. [CrossRef]
26. Bladé, E.; Gómez-Valentín, M.; Dolz, J.; Aragón-Hernández, J.L.; Corestein, G.; Sánchez-Juny, M. Integration of 1D and 2D finite volume schemes for computations of water flow in natural channels. *Adv. Water Resour.* **2012**, *42*, 17–29. [CrossRef]
27. Bladé, E.; Gómez, M.; Sánchez-Juny, M.; Dolz, J. Source term treatment of SWEs using the surface gradient upwind method. *J. Hydraul. Res.* **2012**, *50*, 447–448. [CrossRef]
28. Bermúdez, A.; Dervieux, A.; Desideri, J.-A.; Vázquez, M.E. Upwind schemes for the two-dimensional shallow water equations with variable depth using unstructured meshes. *Comput. Methods Appl. Mech. Eng.* **1998**, *155*, 49–72. [CrossRef]
29. LeVeque, R.L. *Finite Volume Methods for Hyperbolic Problems*; Cambridge University Press: Cambridge, MA, USA, 2002; Volume 31.
30. Toro, E.F. *Riemann Solvers and Numerical Methods for Fluid Dynamics*; Springer: Berlin/Heidelberg, Germany, 2009; Volume 40, ISBN 978-3-540-25202-3.
31. Vázquez-Cendón, M.E. Improved treatment of source terms in upwind schemes for the shallow water equations in channels with irregular geometry. *J. Comput. Phys.* **1999**, *148*, 497–526. [CrossRef]
32. Chevrel, M.O.; Labroquère, J.; Harris, A.J.L.; Rowland, S.K. PyFLOWGO: An open-source platform for simulation of channelized lava thermo-rheological properties. *Comput. Geosci.* **2018**, *111*, 167–180. [CrossRef]
33. Christen, M.; Kowalski, J.; Bartelt, P. RAMMS: Numerical simulation of dense snow avalanches in three-dimensional terrain. *Cold Reg. Sci. Technol.* **2010**, *63*, 1–14. [CrossRef]
34. Eglit, M.; Yakubenko, A.; Zayko, J. A Review of Russian Snow Avalanche Models—From Analytical Solutions to Novel 3D Models. *Geosciences* **2020**, *10*, 77. [CrossRef]
35. Pirulli, M.; Sorbino, G. Assessing potential debris flow runout: A comparison of two simulation models. *Nat. Hazards Earth Syst. Sci.* **2008**, *8*, 961–971. [CrossRef]
36. Stefania, S.; Zugliani, D.; Rosatti, G. Dense snow avalanche modelling with Voellmy rheology: TRENT2D vs. RAMMS2D. In Proceedings of the Vistual Snow Science Workshop—VSSW 2020, Fernie, BC, Canada, 4–6 October 2020.
37. Tan, W.Y. *Shallow Water Hydrodynamics*, 1st ed.; Elsevier Science: Amsterdam, The Netherlands, 1992; ISBN 9780080870939.
38. Bladé, E.; Cea, L.; Corestein, G.; Escolano, E.; Puertas, J.; Vázquez-Cendón, E.; Dolz, J.; Coll, A. Iber: Herramienta de simulación numérica del flujo en ríos. *Rev. Int. Métodos Numér. Cálc. Diseño Ing.* **2014**, *30*, 1–10. [CrossRef]
39. Bladé, E.; Cea, L.; Corestein, G. Modelización numérica de inundaciones fluviales. *Ing. Agua* **2014**, *18*, 68.
40. Cea, L.; Bladé, E. A simple and efficient unstructured finite volume scheme for solving the shallow water equations in overland flow applications. *Water Resour. Res.* **2015**, *51*, 5464–5486. [CrossRef]
41. Cea, L.; Legout, C.; Darboux, F.; Esteves, M.; Nord, G. Experimental validation of a 2D overland flow model using high resolution water depth and velocity data. *J. Hydrol.* **2014**, *513*, 142–153. [CrossRef]

42. Uber, M.; Nord, G.; Legout, C.; Cea, L. How do modeling choices and erosion zone locations impact the representation of connectivity and the dynamics of suspended sediments in a multi-source soil erosion model? *Earth Surf. Dyn.* **2021**, *9*, 123–144. [CrossRef]
43. Aranda, J.Á.; Sánchez-Juny, M.; Sanz-Ramos, M.; Beneyto, C. Design of Drainage Downspouts Systems over a Road Embankment. *Water* **2023**, *15*, 3529. [CrossRef]
44. Aranda, J.Á.; Beneyto, C.; Sánchez-Juny, M.; Bladé, E. Efficient Design of Road Drainage Systems. *Water* **2021**, *13*, 1661. [CrossRef]
45. Cea, L.; Bermúdez, M.; Puertas, J.; Bladé, E.; Corestein, G.; Escolano, E.; Conde, A.; Bockelmann-Evans, B.; Ahmadian, R. IberWQ: New simulation tool for 2D water quality modelling in rivers and shallow estuaries. *J. Hydroinform.* **2016**, *18*, 816–830. [CrossRef]
46. Sañudo, E.; Cea, L.; Puertas, J. Modelling Pluvial Flooding in Urban Areas Coupling the Models Iber and SWMM. *Water* **2020**, *12*, 2647. [CrossRef]
47. Sanz-Ramos, M.; Martí-Cardona, B.; Bladé, E.; Seco, I.; Amengual, A.; Roux, H.; Romero, R. NRCS-CN Estimation from Onsite and Remote Sensing Data for Management of a Reservoir in the Eastern Pyrenees. *J. Hydrol. Eng.* **2020**, *25*, 05020022. [CrossRef]
48. Ruiz-Villanueva, V.; Gamberini, C.; Bladé, E.; Stoffel, M.; Bertoldi, W. Numerical Modeling of Instream Wood Transport, Deposition, and Accumulation in Braided Morphologies Under Unsteady Conditions: Sensitivity and High-Resolution Quantitative Model Validation. *Water Resour. Res.* **2020**, *56*, e2019WR026221. [CrossRef]
49. Ruiz-Villanueva, V.; Mazzorana, B.; Bladé, E.; Bürkli, L.; Iribarren-Anacona, P.; Mao, L.; Nakamura, F.; Ravazzolo, D.; Rickenmann, D.; Sanz-Ramos, M.; et al. Characterization of wood-laden flows in rivers. *Earth Surf. Process. Landf.* **2019**, *44*, 1694–1709. [CrossRef]
50. Sanz-Ramos, M.; López-Gómez, D.; Bladé, E.; Dehghan-Souraki, D. A CUDA Fortran GPU-parallelised hydrodynamic tool for high-resolution and long-term eco-hydraulic modelling. *Environ. Model. Softw.* **2023**, *161*, 105628. [CrossRef]
51. Arbat-Bofill, M.; Bladé, E.; Sánchez-Juny, M.; Niñerola, D.; Dolz, J.; Sanchez-Juny, M.; Niñerola, D.; Dolz, J.; Arbat Bofill, M.; Bladé, E.; et al. Case studies of reservoir sedimentation as a consequence of soil erosion. In *Reservoir Sedimentation*; CRC Press: Boca Raton, FL, USA, 2014; pp. 83–92. ISBN 9781138026759.
52. Bladé, E.; Sanz-Ramos, M.; Dolz, J.; Expósito-Pérez, J.; Sánchez-Juny, M. Modelling flood propagation in the service galleries of a nuclear power plant. *Nucl. Eng. Des.* **2019**, *352*, 110180. [CrossRef]
53. Roe, P. A basis for upwind differentiating of the two dimensional unsteady Euler equations. In *Numerical Methodes for Fluid Dynamics II*; Morton, B., Ed.; Oxford University Press: Oxford, UK, 1986.
54. Bingham, E.C. An investigation of the laws of plastic flow. *Bull. Bur. Stand.* **1916**, *13*, 309–353. [CrossRef]
55. Pastor, M.; Haddad, B.; Sorbino, G.; Cuomo, S.; Drempetic, V. A depth-integrated, coupled SPH model for flow-like landslides and related phenomena. *Int. J. Numer. Anal. Methods Geomech.* **2009**, *33*, 143–172. [CrossRef]
56. Chen, H.; Lee, C.F. Runout Analysis of Slurry Flows with Bingham Model. *J. Geotech. Geoenviron. Eng.* **2002**, *128*, 1032–1042. [CrossRef]
57. Naef, D.; Rickenmann, D.; Rutschmann, P.; McArdell, B.W. Comparison of flow resistance relations for debris flows using a one-dimensional finite element simulation model. *Nat. Hazards Earth Syst. Sci.* **2006**, *6*, 155–165. [CrossRef]
58. Voellmy, A. Über die Zerstörungskraft von Lawinen. *Schweizerische Bauzeitung* **1955**, *73*, 15.
59. Bryant, S.M. *Application of Tailings Flow Analyses to Field Conditions*; University of California: Berkeley, CA, USA, 1983.
60. de' Michieli Vitturi, M.; Esposti Ongaro, T.; Lari, G.; Aravena, A. IMEX_SfloW2D 1.0: A depth-averaged numerical flow model for pyroclastic avalanches. *Geosci. Model Dev.* **2019**, *12*, 581–595. [CrossRef]
61. Jeyapalan, J.K.; Duncan, J.M.; Seed, H.B. Investigation of Flow Failures of Tailings Dams. *J. Geotech. Eng.* **1983**, *109*, 172–189. [CrossRef]
62. Gens, A.; Alonso, E.E. Aznalcóllar dam failure. Part 2: Stability conditions and failure mechanism. *Géotechnique* **2006**, *56*, 185–201. [CrossRef]
63. Alonso, E.E.; Gens, A. Aznalcóllar dam failure. Part 1: Field observations and material properties. *Géotechnique* **2006**, *56*, 165–183. [CrossRef]
64. Alonso, E.E.; Gens, A. Aznalcóllar dam failure. Part 3: Dynamics of the motion. *Géotechnique* **2006**, *56*, 203–210. [CrossRef]
65. Ayala-Carcedo, J. La rotura de la balsa de residuos mineros de Aznalcóllar (España) de 1998 y el desastre ecológico consecuente del río Guadiamar: Causas, efectos y lecciones. *Bol. Geol. Min.* **2004**, *115*, 711–738.
66. Sanz-Ramos, M.; Bladé, E.; Dolz, J.; Sánchez-Juny, M. Revisiting the Hydraulics of the Aznalcóllar Mine Disaster. *Mine Water Environ.* **2022**, *41*, 335–356. [CrossRef]
67. Sanz-Ramos, M.; Bladé, E.; Dolz, J.; Sánchez-Juny, M. El desastre de Aznalcóllar: ¿lodos o aguas ácidas? *Ing. Agua* **2021**, *25*, 229–239. [CrossRef]
68. Consultec Ingenieros SL. Calibración de las tres estaciones de aforo del río Guadiamar (EA nº 56, EA nº 90 y EA nº 76) por métodos informáticos hidráulicos. *Estud. Riada Tóxica* **1999**, *35*.
69. Antón-Pacheco, C.; Arranz, J.C.; Barettino, D.; Carrero, G.; Giménez, M.; Gómez, J.A.; Gumiel, J.C.; López-Pamo, E.; Martín Rubí, J.A.; Martínez-Pledel, B.; et al. Actuaciones para el reconocimiento y retirada de los lodos depositados sobre el terreno, y su restauración edáfica y morfológica. *Bol. Geol. Min.* **2001**, *112*, 93–122.
70. CSIC Guadiamar. *Ciencia, Técnicia y Restauración—El Accidente Minero Diez Años Después*; Consejo Superior de Investigaciones Científicas (CSIC), Ministerio de Ciencia e Innovación: Madrid, Spain, 2008; ISBN 978-84-00-08644-2.

71. Turner, J.N.; Brewer, P.A.; Macklin, M.G. Fluvial-controlled metal and As mobilisation, dispersal and storage in the Río Guadiamar, SW Spain and its implications for long-term contaminant fluxes to the Doñana wetlands. *Sci. Total Environ.* **2008**, *394*, 144–161. [CrossRef] [PubMed]
72. Bladé, E.; Gómez-Valentín, M.; Sánchez-Juny, M.; Dolz, J. Preserving steady-state in one-dimensional finite-volume computations of river flow. *J. Hydraul. Eng.* **2008**, *134*, 1343–1347. [CrossRef]
73. Dimitriadis, P.; Koutsoyiannis, D.; Iliopoulou, T.; Papanicolaou, P. A Global-Scale Investigation of Stochastic Similarities in Marginal Distribution and Dependence Structure of Key Hydrological-Cycle Processes. *Hydrology* **2021**, *8*, 59. [CrossRef]
74. Ramos-Fuertes, A.; Marti-Cardona, B.; Bladé, E.; Dolz, J. Envisat/ASAR Images for the Calibration of Wind Drag Action in the Doñana Wetlands 2D Hydrodynamic Model. *Remote Sens.* **2013**, *6*, 379–406. [CrossRef]
75. Sanz-Ramos, M.; Téllez-Álvarez, J.; Bladé, E.; Gómez-Valentín, M. Simulating the hydrodynamics of sewer-grates using a 2D-hydraulic model. In Proceedings of the 5th International Conference SimHydro, Nice, France, 20–22 November 2019; p. 8.
76. Cea, L.; Puertas, J.; Vázquez-Cendón, M.-E. Depth averaged modelling of turbulent shallow water flow with wet-dry fronts. *Arch. Comput. Methods Eng.* **2007**, *14*, 303–341. [CrossRef]
77. Sanz-Ramos, M.; Olivares, G.; Bladé, E. Experimental characterization and two-dimensional hydraulic-hydrologic modelling of the infiltration process through permeable pavements. *Rev. Int. Métodos Numér. Cálc. Diseño Ing.* **2022**, *38*, 1–12. [CrossRef]
78. Msheik, K. *Non–Newtonian Fluids: Modeling and Well-Posedness*; Universite Grenoble Alpes: Saint-Martin-d'Hères, France, 2020.
79. Takahashi, T. Debris flow: Mechanics and hazard mitigation. In *Proceedings of the ROC-JAPAN Joint Seminar on Multiple Hazards Mitigation*; National Taiwan Univerisity: Taipei, Taiwan, 1985; pp. 1075–1092.
80. Laenen, A.; Hansen, R.P. *Simulation of Three Lahars in the Mount St. Helens Area, Washington, Using a One-Dimensional, Unsteady-State Streamflow Model*; U.S. Geological Survey Water-Resources Investigations Report 88-4004; U.S. Geological Survey: Portland, OR, UA, 1988.
81. Syarifuddin, M.; Oishi, S.; Hapsari, R.I.; Legono, D. Empirical model for remote monitoring of rain-triggered lahar at Mount Merapi. *J. Japan Soc. Civ. Eng. Ser. B1 (Hydraul. Eng.)* **2018**, *74*, I_1483–I_1488. [CrossRef] [PubMed]
82. Darnell, A.R.; Phillips, J.C.; Barclay, J.; Herd, R.A.; Lovett, A.A.; Cole, P.D. Developing a simplified geographical information system approach to dilute lahar modelling for rapid hazard assessment. *Bull. Volcanol.* **2013**, *75*, 713. [CrossRef]
83. Macedonio, G.; Pareschi, M.T.T. Numerical simulation of some lahars from Mount St. Helens. *J. Volcanol. Geotherm. Res.* **1992**, *54*, 65–80. [CrossRef]
84. O'Brien, J.S.; Julien, P.Y. Laboratory Analysis of Mudflow Properties. *J. Hydraul. Eng.* **1988**, *114*, 877–887. [CrossRef]
85. Bartelt, P.; Valero, C.V.; Feistl, T.; Christen, M.; Bühler, Y.; Buser, O. Modelling cohesion in snow avalanche flow. *J. Glaciol.* **2015**, *61*, 837–850. [CrossRef]
86. Kelfoun, K. Suitability of simple rheological laws for the numerical simulation of dense pyroclastic flows and long-runout volcanic avalanches. *J. Geophys. Res. Solid Earth* **2011**, *116*, 1–14. [CrossRef]
87. Frattini, P.; Crosta, G.B.; Fusi, N.; Dal Negro, P. Shallow landslides in pyroclastic soils: A distributed modelling approach for hazard assessment. *Eng. Geol.* **2004**, *73*, 277–295. [CrossRef]
88. de Bélizal, E.; Lavigne, F.; Hadmoko, D.S.; Degeai, J.-P.; Dipayana, G.A.; Mutaqin, B.W.; Marfai, M.A.; Coquet, M.; Le Mauff, B.; Robin, A.-K.; et al. Rain-triggered lahars following the 2010 eruption of Merapi volcano, Indonesia: A major risk. *J. Volcanol. Geotherm. Res.* **2013**, *261*, 330–347. [CrossRef]
89. Dumaisnil, C.; Thouret, J.; Chambon, G.; Doyle, E.E.; Cronin, S.J.; Surono. Hydraulic, physical and rheological characteristics of rain-triggered lahars at Semeru volcano, Indonesia. *Earth Surf. Process. Landf.* **2010**, *35*, 1573–1590. [CrossRef]
90. Pistolesi, M.; Cioni, R.; Rosi, M.; Cashman, K.V.; Rossotti, A.; Aguilera, E. Evidence for lahar-triggering mechanisms in complex stratigraphic sequences: The post-twelfth century eruptive activity of Cotopaxi Volcano, Ecuador. *Bull. Volcanol.* **2013**, *75*, 698. [CrossRef]
91. van Westen, C.J.; Daag, A.S. Analysing the relation between rainfall characteristics and lahar activity at Mount Pinatubo, Philippines. *Earth Surf. Process. Landf.* **2005**, *30*, 1663–1674. [CrossRef]
92. Manville, V.; Major, J.J.; Fagents, S.A. Modeling lahar behavior and hazards. In *Modeling Volcanic Processes: The Physics and Mathematics of Volcanism*; Fagents, S.A., Gregg, T.K.P., Lopes, R.M.C., Eds.; Cambridge University Press: Cambridge, UK, 2013; pp. 300–330.
93. WISE. Chronology of Major Tailings Fam Failures. WISE Uranium Project Is Part of World Information Service on Energy. 2020. Available online: https://www.wise-uranium.org/mdaf.html (accessed on 15 July 2024).
94. Penman, A.D.M.; Brook, D.; Martin, P.L.; Routh, D. *Tailings Dams. Risk of Dangerous Occurrences. Lessons Learnt from Practical Experiences*; Commission Internationale des UNEP/ICOLD: Paris, France, 2001; Volume 121, ISBN 9783540773405.
95. Capart, H.; Eldho, T.I.; Huang, S.Y.; Young, D.L.; Zech, Y. Treatment of Natural Geometry in Finite Volume River Flow Computations. *J. Hydraul. Eng.* **2003**, *129*, 385–393. [CrossRef]
96. Hou, J.; Liang, Q.; Simons, F.; Hinkelmann, R. A stable 2D unstructured shallow flow model for simulations of wetting and drying over rough terrains. *Comput. Fluids* **2013**, *82*, 132–147. [CrossRef]
97. Pitman, E.B.; Nichita, C.C.; Patra, A.; Bauer, A.; Sheridan, M.; Bursik, M. Computing granular avalanches and landslides. *Phys. Fluids* **2003**, *15*, 3638–3646. [CrossRef]
98. Mergili, M.; Fischer, J.T.; Krenn, J.; Pudasaini, S.P. r.avaflow v1, an advanced open-source computational framework for the propagation and interaction of two-phase mass flows. *Geosci. Model Dev.* **2017**, *10*, 553–569. [CrossRef]

99. Courant, R.; Friedrichs, K.; Lewy, H. On the partial difference equations of mathematical physics. *IBM J. Res. Dev.* **1967**, *11*, 215–234. [CrossRef]
100. Buttinger-Kreuzhuber, A.; Konev, A.; Horváth, Z.; Cornel, D.; Schwerdorf, I.; Blöschl, G.; Waser, J. An integrated GPU-accelerated modeling framework for high-resolution simulations of rural and urban flash floods. *Environ. Model. Softw.* **2022**, *156*, 105480. [CrossRef]
101. Carlotto, T.; Borges Chaffe, P.L.; Innocente dos Santos, C.; Lee, S. SW2D-GPU: A two-dimensional shallow water model accelerated by GPGPU. *Environ. Model. Softw.* **2021**, *145*, 105205. [CrossRef]
102. Dehghan-Souraki, D.; López-Gómez, D.; Bladé-Castellet, E.; Larese, A.; Sanz-Ramos, M. Optimizing sediment transport models by using the Monte Carlo simulation and deep neural network (DNN): A case study of the Riba-Roja reservoir. *Environ. Model. Softw.* **2024**, *175*, 105979. [CrossRef]
103. Klose, C.D. Mine Water Discharge and Flooding: A Cause of Severe Earthquakes. *Mine Water Environ.* **2007**, *26*, 172–180. [CrossRef]

Disclaimer/Publisher's Note: The statements, opinions and data contained in all publications are solely those of the individual author(s) and contributor(s) and not of MDPI and/or the editor(s). MDPI and/or the editor(s) disclaim responsibility for any injury to people or property resulting from any ideas, methods, instructions or products referred to in the content.